15TH IEA HEAT PUMP CONFERENCE
MAY 26–29, 2026 | HOFBURG
VIENNA 2026
DECARBONISATION THROUGH INNOVATION

Application of a Phase-Change Material Heat Exchanger to Improve the Efficiency of Air-conditioners at Partial Loads

Koharu Tani[a], Sayaka Kindaichi[a*], Keita Kawasaki[b]

[a]Graduate School of Advanced Science and Engineering, Hiroshima University, Higashihiroshima 739-8527, Japan
[b]Department of Architecture and Structural Engineering, National Institute of Technology (KOSEN), Kure College, Kure 737-8506, Japan.

Abstract

Inverter-equipped air conditioning (AC) systems offer variable speed control allowing for increased energy efficiency. However, AC systems often operate at low load ratios below where inverter control is effective, which reduces their energy efficiency. We developed an AC system that increases the apparent load ratio of the compressor in cooling seasons by using a phase-change material (PCM) as a high-performance heat exchanger. PCM cooling and heating experiments were conducted with a PCM heat exchanger, which comprised aluminum plates and fins filled with 0.8 kg of paraffinic PCM with a phase change temperature of 17°C–18°C. The outlet air temperature was close to the phase change temperature during both the PCM cooling and heating experiments, indicating a high heat transfer coefficient of >70 W/(m^2·K). A simplified numerical model of the PCM heat exchanger as a lumped constant system was created using the experimentally obtained coefficient. A parametric study revealed that the effective weight for heat exchange was 5.83 kg for aluminum and 0.53 kg for PCM. The calculations generally reproduced the experimental results, with root mean squared errors of 0.39 K for PCM cooling and 0.84 K for PCM heating, confirming their accuracy. Simulations were then conducted comparing the energy performance of the proposed system to that of a system without PCM in an office space for the cooling season. While low load operation accounted for 39% of the total AC time for a non-PCM system, it was reduced to 2.7% for the proposed system. The proposed system demonstrated load ratios of 50%–60% for most of the cooling season and achieved a high coefficient of performance. The PCM heat exchanger reduced energy consumption by 11% in the whole cooling season, owing to the improved efficiency at partial load ratios.

Keywords: inverter heat pumps; energy efficiency; phase change materials (PCMs); PCM heat exchanger; heat transfer coefficient; numerical model; energy consumption

1. Introduction

While the promotion of renewable energy sources is important for achieving carbon neutrality, an equally necessary step is improving energy efficiency on the demand side through the use of air conditioning (AC) systems [1]. In Japan, AC systems are commonly equipped with inverters, which offer variable speed control so that the AC system can operate efficiently not only at large load ratios close to the compressor capacity but also at partial load ratios [2]. However, inverter control becomes invalid at small load ratios below ~20% during which the compressor is simply turned on or off as necessary, which is inefficient [3]. During actual operation, AC systems tend to be at low load ratios because they are generally designed with excess capacity so that they can sufficiently cool and heat buildings during even the hottest and coldest days throughout the year. We performed field measurements showing that the energy efficiency of AC systems in actual residential buildings decreases at low load ratios [4,5]. Therefore, it is necessary to improve the energy efficiency of AC

* Corresponding author. Tel.: +81-82-424-7832
E-mail address: kindaichi@hiroshima-u.ac.jp

systems at low load ratios below the lower limit of inverter control to further reduce the energy consumption and CO_2 emissions of AC systems.

Thermal energy storage (TES) is a technology that can be used to adjust the temporal gap between energy supply and demand, which tend to peak at different times [6]. Unlike general sensible heat storage, in which water or concrete is utilized as the storage medium, phase-change materials (PCMs) can charge or discharge large amounts of heat at a constant temperature when they change phase [6]. Various studies have explored applying PCMs to buildings, such as mixing PCMs with flooring, wall, and roof materials, to extend the thermal capacity of buildings and stabilize the indoor thermal environment [7–9] or encapsulating PCMs in radiation panels to function as part of a thermally activated building structure [10,11]. Many studies have utilized PCMs to store natural thermal energy, such as solar heat [12,13] or cool air at night [14–16], to reduce the load and energy consumption of AC systems. Several studies have investigated precooling or prewarming PCMs at night, during which the energy supply tends to exceed demand, as a load leveling or peak shaving strategy [17,18]. Some researchers have proposed applications for PCMs in which AC systems operate during energy-efficient hours, such as in the early morning in warm regions [19] and in the daytime in cold regions [20]. However, few studies have considered applying PCMs to improve the energy efficiency of inverter-equipped AC systems at low load ratios.

The practical application of PCMs requires an increase in the heat transfer coefficient of the PCM itself or a heat exchanger. Several studies have reported that adding nanoparticles increases the apparent heat conductivity of a PCM [21]. Several researchers have investigated the heat exchange characteristics of functional PCMs enclosed in shell-and-tube type heat exchangers [22], triple tube heat exchangers [23], and porous foam materials forming wavy air channels [24]. While shell-and-tube type heat exchangers are commonly used for PCM applications where heat is exchanged with water [25], different heat exchangers have been investigated for buildings where heat is exchanged with air [26,27], such as the tube type [28], ball type [29], plate type [30], and finned plate type [31]. We also investigated using a packed bed of granulated PCM as a heat exchanger [32,33]. Although the granulated PCM had a large surface area that resulted in a large heat transfer coefficient with air, problems remained in terms of sealing and pressure drop for use in actual AC systems. Thus, research has been insufficient on PCM applications where heat is exchanged with air that achieve both a high thermal performance and a low pressure drop.

In this study, we utilized the TES concept through a high-performance PCM heat exchanger to operate a AC system at a high apparent load ratio and avoid low-efficiency intermittent operation in the cooling season. To evaluate the effectiveness of our design, we fabricated a prototype heat exchanger containing about 1 kg of PCM and conducted experiments to observe the heat exchange characteristics and pressure loss at different air flow rates. Numerical simulations were carried out to evaluate the energy efficiency of the proposed AC system in different months and at partial load ratios compared to a conventional AC system without TES.

2. Design

Figure 1 shows conceptual diagrams of the proposed AC system in charge and discharge modes. A PCM heat exchanger is connected to the indoor unit, which is installed in a ceiling space with air ducts. In this study, we investigated the use of this AC system for space cooling operations in summer. In charge mode, air taken from the room is first cooled in the indoor unit, which acts as an evaporator in the refrigeration cycle. The air then passes through the PCM heat exchanger, which cools the PCM inside and is returned to the room as conditioned air. The air flow rate of the fan in the indoor unit is varied to remove the cooling load in the room and to cool the PCM within the rated value. Because the room and PCM are cooled simultaneously, the load ratio of the outdoor unit is increased, which increases the energy efficiency ratio (EER). In discharge mode, the fan in the indoor unit contributes to ventilation rather than the refrigeration cycle. The air taken from the room is cooled by the PCM heat exchanger and circulated back to the room to remove the cooling load. The charge and discharge modes switch according to the outlet temperature (T_{out}) under the assumption that the PCM completes the phase change.

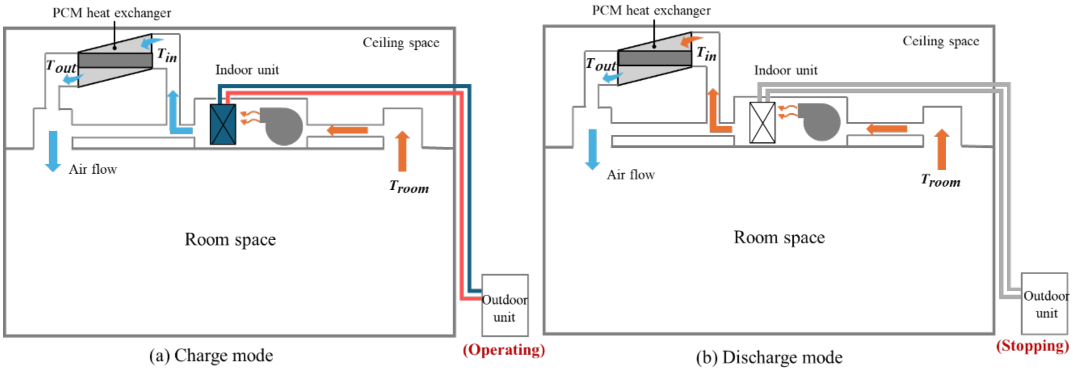

Figure 1. Schematic diagrams of the proposed AC system in (a) charge and (b) discharge modes.

3. Experimental setup

Figures 2 and 3 show the dimensions and schematic diagrams, respectively, of the PCM heat exchanger prototype. The prototype was made of aluminum with a weight of 8.9 kg and external dimensions of 235 × 300 × 374 mm. Air passes through the heat exchange element filled with PCM (shaded in orange). The heat exchange element consisted of aluminum plates connected by aluminum fins. The 1 mm-thick aluminum plates had a hollow structure, with additional mesh-like fins arranged inside. The total heat exchange area was 4 m^2. Air exchanges heat with the heat exchange element by passing between the fins. PCM temperature (T_p) was measured at the junction of the PCM filling sections, as shown in Fig. 3b, because of the limited space for inserting a thermocouple. Table 1 presents the physical properties of the PCM used to fill the heat exchange element. The PCM mainly consisted of paraffin wax. Differential scanning calorimetry of a 1.7 mg sample determined the melting and solidification temperatures as 17.8 and 17 °C, respectively. The amount of latent heat was determined as 188 kJ/kg. The PCM was enclosed in the heat exchange element in liquid form with a filling weight of 0.8 kg.

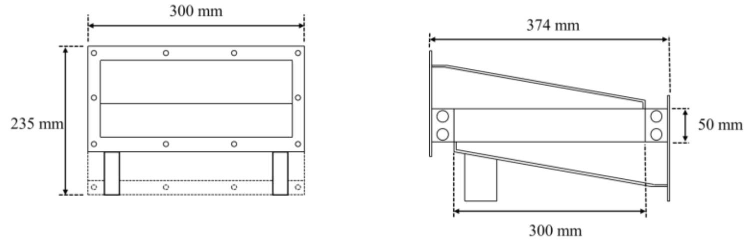

Figure 2. Dimensions of the PCM heat exchanger.

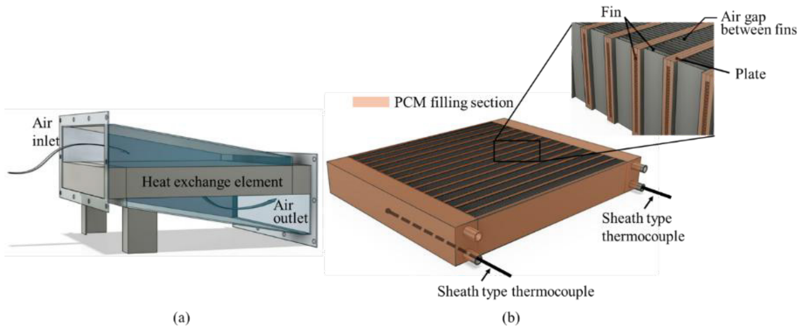

Figure 3. Schematic diagrams of the PCM heat exchanger: (a) overall appearance and (b) enlarged view of the heat exchange element.

Table 1. Physical properties of the PCM.

Physical Properties	Value
Latent heat amount	188 kJ/kg
Melting point	17.8 °C
Freezing point	17.0 °C

Figure 4 shows a schematic diagram of the experimental system, including an exterior view. Air ducts were connected in front of and behind the PCM heat exchanger with plastic guides installed in the front duct to regulate the air. A chilled/warmed water coil and a fan were installed at the inlet and outlet of the air duct. The water in the coil was controlled to a specific temperature by a constant-temperature chiller. The PCM heat exchanger was covered with thermal insulation during the experiment. Figure 5 shows the measurement points, while Table 2 presents the specifications of the measurement devices and sensors. The temperature, differential pressure, and wind speed were measured every 30 s. The inlet air temperature (T_{in}) and outlet air temperature (T_{out}) were measured by thermocouples placed at nine points near the front and back surfaces, respectively, of the fins. The differential pressure was measured before and after the heat exchange element. The air velocity was measured by a one-dimensional hot-wire anemometer placed at the center of the duct cross-section. An air filter that straightened air flow was set upstream in the duct to ensure uniform airflow distribution as shown in Fig 5. The air velocity at the center of the duct cross-section was confirmed to be representative, as the gap between the air velocity at the center of the duct and the average air velocity across the duct cross-section was less than 10%.

Experiments were performed to evaluate first the PCM cooling process and then the PCM heating process. For the PCM cooling process, the PCM was solidified, and the T_{in} was controlled at 10 °C by using chilled water, which was set at 5 °C in the coil. The PCM cooling process was completed once the PCM temperature (T_p) dropped below 12 °C. For the PCM heating process, T_{in} was increased to 30 °C by the chiller under the assumption that air passing through the heat exchanger is cooled by the PCM in ventilation mode without the aid of the compressor. The PCM heating process continued until T_p > 20 °C, at which point the PCM was completely melted.

Table 3 presents the experimental cases 1–3. The air velocity was set to 0.5, 1.0, and 1.5 m/s, respectively, by adjusting the fan frequency. The air flow rate was calculated as the product of the measured air velocity and cross-sectional area and was 32, 64, and 95 m^3/h, respectively. Each case was tested at least twice between May and July 2024.

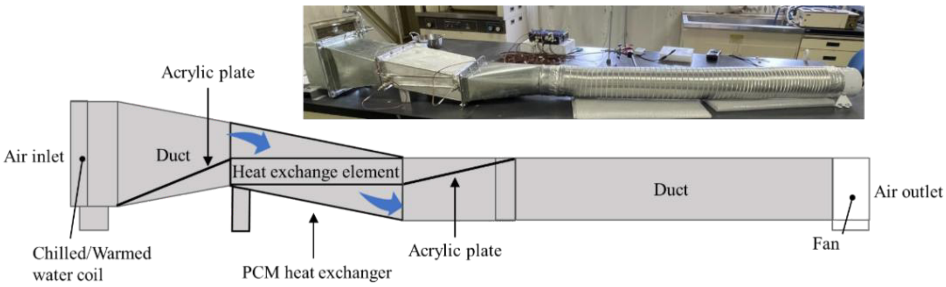

Figure 4. Schematic diagrams of the experimental system.

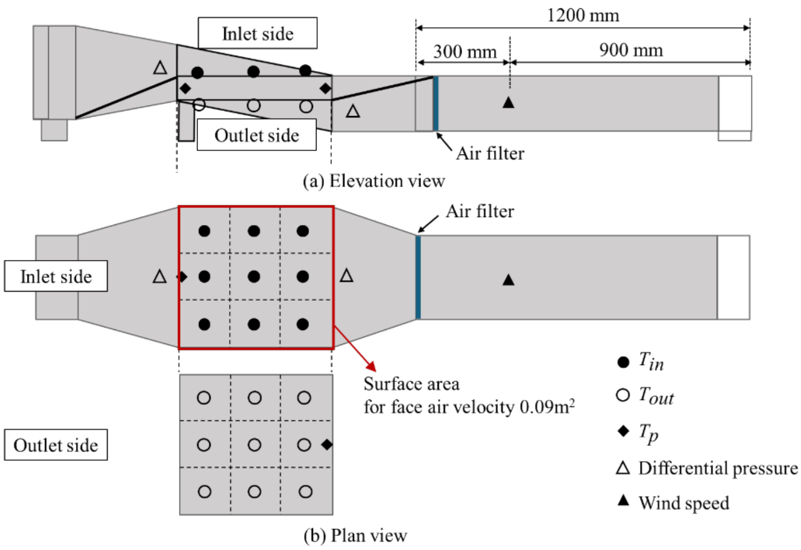

Figure 5. Measurement points: (a) elevation view and (b) plan view.

Table 2. Measurement devices and sensors.

Measurement Item	Device	Sensors	Range	Accuracy
Air temperature	HIOKI data logger*1	Thermocouples [Type T, Class1]	~100 °C	±0.5 °C
PCM temperature	HIOKI data logger*1	Thermocouples sheath type	−200 to +300 °C	±0.5 °C
Air velocity	Testo480 multifunction measuring instrument*2	Testo Hot-wire anemometer	0 to 20 m/s	±0.03 m/s
Pressure loss	OMRON differential pressure station*3		−500 to 500 Pa	±0.2 Pa

Manufacturer information: *1 HIOKI E.E. CORPORATION (Nagano, Japan), *2 Testo SE & Co. KGaA (Titisee-Neustadt, Germany), *3 OMRON Corporation (Kyoto, Japan)

Table 3. Experimental cases.

Properties	Case 1	Case 2	Case 3
Air velocity [m/s]	0.5	1.0	1.5
Air flow rate [m^3/h]	32	64	95

4. Identification of overall heat transfer coefficient

The amount of heat exchanged by the PCM heat exchanger (Q) was calculated as follows:

$$Q = c_a \rho_a V (T_{in} - T_{out}) \tag{1}$$

where c_a is the specific heat of air [kJ/(kg·K)], ρ_a is the density of air [kg/m^3], and V is the air flow rate [m^3/s]. V, T_{in}, and T_{out} were measured in the experiments. T_{in} and T_{out} are the mean of the values obtained at the nine measurement points on each side of the heat exchange element. Equation (1) represents only sensible heat transfer based on air temperature changes, assuming that no dehumidification occurs in the PCM heat exchanger. The overall heat transfer coefficient (U) was calculated as follows:

$$U = Q/(A_{ex} \times \Delta T) \tag{2}$$

where A_{ex} is the heat exchange area [m^2], and ΔT is the difference between T_p and T_{out} [K]. Both the gap between T_p and T_{in} and the gap between T_p and T_{out} could be used to define ΔT. However, the gap between T_p and T_{in} indicates only the potential driving force of heat transfer whereas the gap between T_p and T_{out} indicates the actual result of heat transfer. Therefore, ΔT was defined using T_p and T_{out}.

Figure 6 shows the relationship between the face air velocity and pressure drop in the heat exchange element. The face air velocity was calculated by dividing V by 0.09 m^2, which is the surface area of the heat exchange element. At a face air velocity of 0.1–0.3 m/s, the pressure drop was only 2–9 Pa and was generally below 10 Pa. This pressure drop is much smaller than that of typical fin-tube heat exchangers, which require a face air velocity of approximately 3.0 m/s to achieve U values of 55–60 W/(m^2·K) [35].

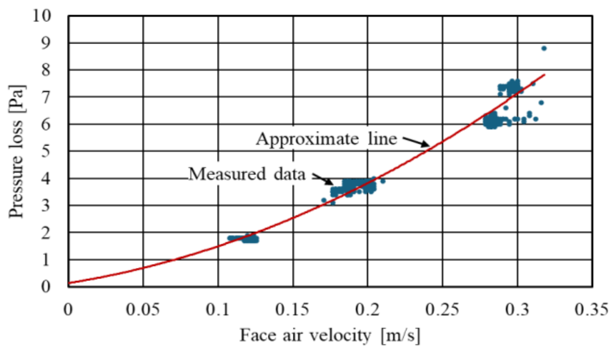

Figure 6. Relationship between the face air velocity and pressure drop in the PCM heat exchanger.

To predict T_{out} after the heat exchange, we formulated empirical formulas for calculating U based on the experimental results. Figure 7 shows the relationships between T_p and U obtained in the PCM cooling and heating processes. The values observed every 30 s are plotted on the figure. Large values of U were observed at temperatures of 17 and 18 °C, which correspond to the phase change temperature of the PCM. During the PCM cooling process, U was 10–20 W/(m^2·K) above the phase change temperature and increased sharply when T_p was below 18 °C. U became small again below the phase change temperature with an average value of 4.1 W/(m^2·K). During the PCM heating process, U was around 20 W/(m^2·K) below the phase change temperature and increased drastically when T_p exceeded 17 °C. While U decreased to 10 W/(m^2·K) after the phase change, it rose again in several cases, which may be due to the melting of the PCM deep inside the heat exchange element.

During the phase change, the relationship between U and T_p can be approximated as a power law that asymptotically approaches 17.57 °C during the PCM cooling process and 17.60 °C during the PCM heating process, where a bi-square weighting function is applied to prevent the influence of outliers.

$$U_{PCM\ charge} = 16.17\left(T_p - 17.57\right)^{-0.31}. \tag{3}$$

$$U_{PCM\ discharge} = 24.80\left(17.60 - T_p\right)^{-0.24}. \tag{4}$$

When compared with the experimental results, both Equations (3) and (4) showed a high explanatory power with $R^2 > 0.7$.

After the phase change, U decreased linearly from the maximum U value with a temperature difference of 0.2 K to constant values of 4.1 W/(m^2·K) during the PCM cooling process and 9.5 W/(m^2·K) during the PCM heating process, on average.

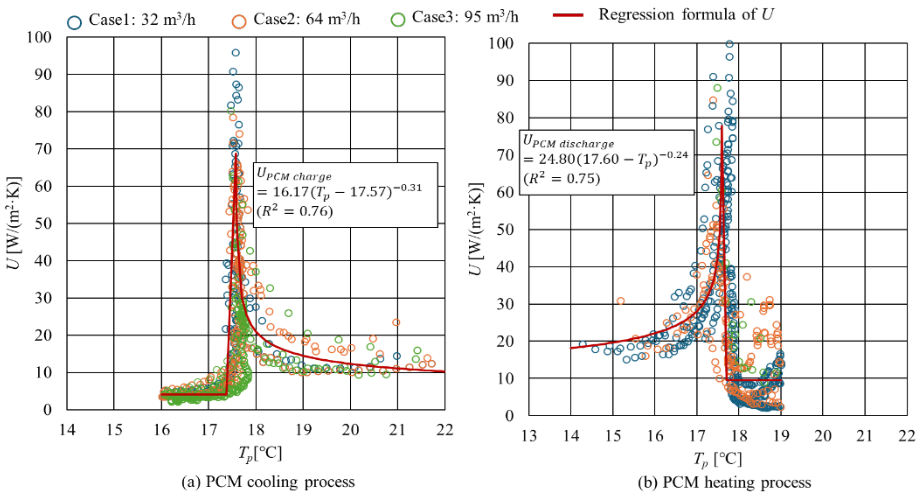

Figure 7. Relationship between T_p and U during (a) PCM cooling and (b) PCM heating processes.

5. Numerical Model

A numerical model was developed to predict T_{out} from the PCM heat exchanger. The temperature distribution in the PCM heat exchanger was not considered under the assumption that the air flow is uniform across the cross-section. The heat balance in the PCM heat exchanger can then be represented as a lumped constant system where the internal PCM and exterior aluminum are a single unit:

$$\left(W_{ale} + W_{pe}\right)\frac{dH_{p+al}}{dt} = UA_{ex}\left(T_{out} - T_p\right) \tag{5}$$

where W_{pe} and W_{ale} are the effective weights of the PCM and aluminum [kg], respectively, contributing to the heat exchange. The heat capacity of the PCM heat exchanger can be expressed as the change in enthalpy per the total effective weight of PCM and aluminum (H_{p+al}) [kJ/kg]. H_{p+al} can be converted to T_p by the enthalpy method. The amount of heat exchanged with air can then be calculated by using U as determined from the experimental results. The heat balance on the air side can be represented by the heat from advection and heat exchanged by the PCM heat exchanger:

$$c_a \rho_a V(T_{out} - T_{in}) = UA_{ex}(T_p - T_{out}) + Q_{loss} \quad (6)$$

where the heat storage of air can be neglected as its heat capacity was sufficiently smaller than that of the PCM heat exchanger. Equation (6) can then be used to determine T_{out}. Q_{loss} is the heat loss and is calculated as follows:

$$Q_{loss} = K_{loss} A_{sur} (\frac{T_{in} + T_{out}}{2} - T_{amb}) \quad (7)$$

where K_{loss} is the heat loss coefficient identified as 2.0 W/(m^2·K) from experimental validation, A_{sur} is the surface area of the PCM heat exchanger (=4.0) [m^2], and T_{amb} is the ambient air temperature [°C].

Figure 8 shows the relationship between temperature and enthalpy for the combined mass of PCM and aluminum as given by the enthalpy method. The latent heat due to the phase change of the PCM can be obtained from the linear relationship at 17–18 °C. The enthalpy change outside the phase change temperature can be calculated by using the mean specific heat of the PCM heat exchanger:

$$c_{p+al} = (W_{pe} \times c_p + W_{ale} \times c_{al})/(W_{pe} + W_{ale}) \quad (8)$$

where c_{p+al}, c_p, and c_{al} are the specific heats of the PCM heat exchanger, PCM, and aluminum [kJ/(kg·K)].

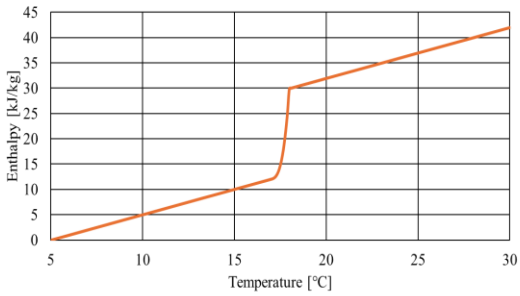

Figure 8. Relationship between temperature and enthalpy per the total mass of PCM and aluminum

Due to the delay in melting of PCM deep in the heat exchanger observed in the experiment, the PCM in the junction may have been partially delayed or not contributed to the heat exchange. To represent the phenomenon in the model, W_{pe} and W_{ale} were determined to be 0.53 kg and 5.83 kg, respectively, based on a parametric analysis in the previous study [34].

The accuracy of the numerical model was verified under the same boundary conditions as in the experiment, using W_{ale} and W_{pe}, as determined previously. Figure 9 shows the relationship between the experimental and calculated T_{out}. The calculated T_{out} was sometimes higher than the experimental T_{out} during the PCM cooling and lower during the PCM heating process. The calculated T_{out} generally remained constant while the experimental T_{out} varied under the influence of T_{in}. Deviations were observed in cases 1 and 2, which had relatively small air volumes. The experimental results suggested that the phase change occurred in a distributed manner in the prototype, but the numerical model assumed that the heat exchanger was a lumped constant system. This had the clear effect of regulating the temperature during the phase change in the calculated results compared with the experimental observations. In cases with a smaller air volume, the phase change progressed more slowly, which may have facilitated the dispersion of heat extracted from the PCM to the air during the experiment. Overall, the average RMSE for all cases was 0.39 K for the PCM cooling process and 0.84 K for the PCM heating process, indicating relatively good reproducibility. Thus, the numerical model showed reasonable accuracy for evaluating seasonal or annual system behaviours despite its simplicity. Further validation may be needed with modified heat exchangers that reflect the ideal heat exchange behavior of a lumped constant system.

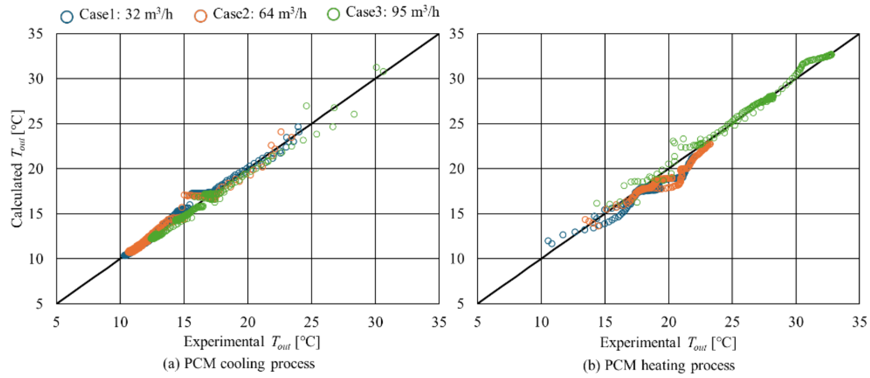

Figure 9. Relationship between experimental and calculated values of T_{out} during (a) PCM cooling and (b) PCM heating processes.

6. Simulations

6.1. Conditions

Energy simulations were performed by applying the developed numerical model to an office space with windows on the south side, as shown in Fig 10. An AC system was constructed by using the Life Cycle Energy Management (LCEM) tool ver. 3.10 distributed by MLIT [36]. The system was assumed to be a variable refrigerant flow (VRF) system comprising eight indoor units and one outdoor unit, where a PCM heat exchanger was connected to each indoor unit. The energy consumption was calculated at 5 min intervals by using cooling loads from May 1 to October 31 obtained from the Building Energy Simulation Tool (BEST) Program [37] as the input. The weather data in Tokyo, standard values of heat gains through structure and windows, and internal loads were used to calculate the cooling load. Table 4 presents the specifications of the AC system, which were determined so that the outdoor unit operated at an average load ratio in July of 30% for Case 1 and 20% for Case 2. The eight indoor units were assumed to exhibit the same behavior, and the set of one indoor unit and PCM heat exchanger shared one-eighth of the cooling load. The required weight of PCM was determined to be 4.24 kg for each PCM heat exchanger by a parametric study [34]. The inlet air temperature to the PCM heat exchanger (T_{in}) and air flow rate (V) as determined by the cooling load were used as inputs to calculate the outlet air temperature from the PCM heat exchanger (T_{out}). The charge and discharge modes were switched based on T_{out}, as shown in Fig 1. In charge mode, the outdoor unit was operated to cool the room space and the PCM at the same time. When T_{out} fell below 15 °C, the system switched to discharge mode, in which the room space was cooled by the charged PCM, and the outdoor unit did not operate. When T_{out} rose above 21 °C, the system switched back to charge mode.

Table 4. Specifications of the AC system

(a) Outdoor unit

	Case 1	Case 2
Number of outdoor units	1	1
Rated cooling capacity [kW]	65	97.5
Rated power consumption [kW]	17.8	26.8
Rated EER (SEER)	3.64 (4.8)	3.64 (5.2)

(b) Indoor unit

	Case 1	Case 2
Number of outdoor units	8	8
Rated cooling capacity [kW]	7.3	9.0
Rated power consumption [kW]	0.3	0.46
Rated air volume [m³/h]	1170	1800

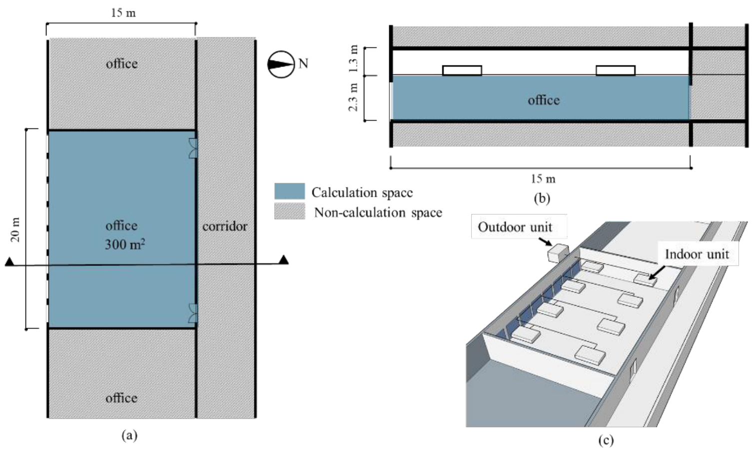

Figure 10. Office model used in the energy simulation; (a) elevation view, (b) plan view, and (c) 3D view.

6.2. Effects of the PCM Heat Exchanger

Figures 11 show the load ratio frequencies at 10% intervals and the EER for each load ratio of the outdoor unit during the whole cooling season in Case 1, with and without PCM. EER was calculated as follows:

$$EER = Q_{outdoor}/E_{outdoor} \tag{9}$$

Where $Q_{outdoor}$ is cooling capacity provided by the outdoor unit [kW] and $E_{outdoor}$ is energy consumption of outdoor unit [kW]. Load ratio was calculated as follows:

$$Load\ ratio = Q_{load}/Q_{rated} \tag{10}$$

where Q_{rated} is rated cooling capacity of the outdoor unit [kW] and Q_{load} is cooling load in the room calculated from the enthalpy difference between supply air and return air of indoor units [kW]. Without PCM, low load ratios of <20% (EER < 3.4) accounted for 680 h, which was 39% of the total AC time. With PCM, low load ratios of <20% were reduced to 2.7% of the total AC time. Instead, the load ratio increased to 50–60% during most of the AC time, resulting in an improved EER of 5.4. Seasonal EER (SEER) with PCM reached 4.97, which was 19% higher than that without PCM. Thus, the PCM heat exchanger clearly helped increase the load ratio of the AC system and achieve a high energy efficiency. Figure 11 (c) shows the monthly energy consumption of the whole AC system including the outdoor and indoor units with and without PCM in Case 1. With PCM, the energy consumption was reduced in all months. During the peak load months of July and August, the cooling capacity of the outdoor unit was insufficient to cool the PCM, leading to relatively small energy-saving effect. The total energy consumption for the cooling season was reduced by 11%, from 6479 kWh without PCM to 5740 kWh with PCM. Additionally, only 0.51% of the required cooling load remained unprocessed. This indicates that the PCM heat exchanger effectively improved the partial load efficiency of the AC system while maintaining thermal comfort.

Similarly, Figures 12 show the result in Case 2 with and without PCM. Case 2 had larger cooling capacity than Case 1, thus without PCM, low load ratios of <20% (EER < 3.2) accounted for 1220 h, which was 69% of the total AC time. The use of PCM reduced the low-load operation to 6.7%, and increased efficient operation at load ratios of 50–60% (EER = 5.4). SEER with PCM was 4.96, which was 32% higher than that without PCM. The total energy consumption was reduced by 30%, from 7850 kWh without PCM to 5533 kWh with PCM. As a result, the monthly energy consumption was reduced in every month by the application of PCM, where energy saving effects equivalent to other months were achieved even during the peak load months of July and August, unlike Case 1. This is mainly because the cooling capacity of the outdoor unit was enough to cool the PCM throughout the season. As in Case 1, the unprocessed cooling load was very small, accounting for only 0.11% of the required cooling load, indicating thermal comfort is maintained.

Comparing Case 1 and Case 2, the SEER increase rate due to PCM application was higher in Case 2 than in Case 1. This is because in Case 2, which had a larger cooling capacity, under normal situations without PCM, inefficient low-load operation may account for a larger proportion than in Case 1. By applying PCM, most of such inefficient operation was shifted to efficient operation, resulting in a greater improvement of SEER in Case 2 than in Case 1. Simultaneously, Case 2 indicated larger energy reduction effects than in Case 1. These results suggest that the PCM application investigated in this study is particularly effective in situations where relatively large-capacity AC systems are installed and low-load operation is likely to occur.

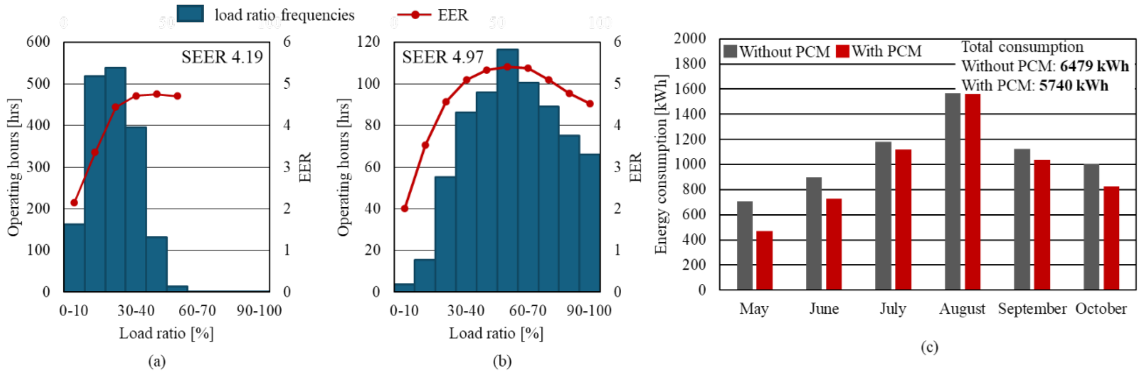

Figure 11. Frequency of load ratios and their average EERs (a) without PCM, (b) with PCM, and (c) monthly energy consumption with and without PCM (Case 1: outdoor unit: 65 kW, indoor unit: 7.3 kW).

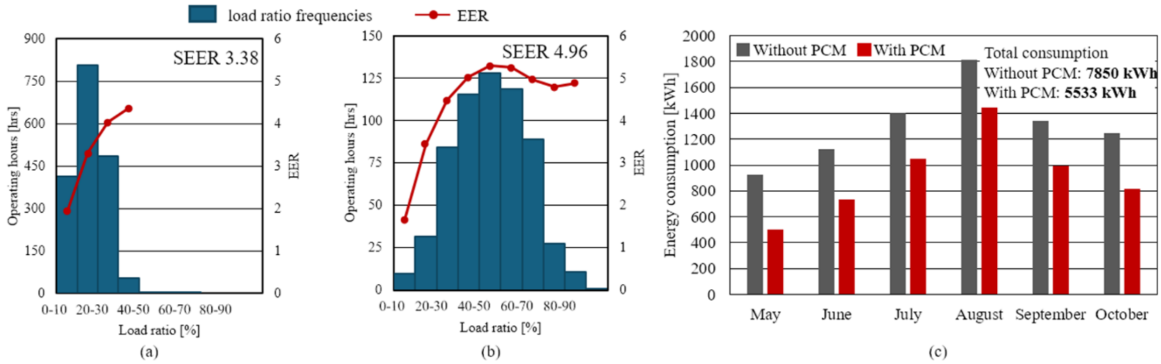

Figure 12. Frequency of load ratios and their average EERs (a) without PCM, (b) with PCM, and (c) monthly energy consumption with and without PCM (Case 2: outdoor unit: 97.5 kW, indoor unit: 9.0 kW).

7. Conclusions

We developed a new AC system that uses a PCM heat exchanger to increase the apparent load ratio of the compressor. Experiments with a prototype heat exchanger demonstrated that the heat exchanger achieved high U value. The heat exchange element also achieved a small pressure drop of less than 10 Pa, suggesting that the PCM heat exchanger could obtain a high thermal performance while maintaining a small pressure drop. The relationship of U to T_p during phase change was formulated as power-law approximations with $R^2 > 0.7$ for both the PCM cooling and heating processes. Currently, U is calculated from T_{out}, which is the output obtained from the experiment. It will be necessary for future work to provide more physical explanations of the relationship with the input conditions.

A numerical model was developed for predicting the outlet air temperature of the PCM heat exchanger. The numerical model was then used in simulations to compare the energy consumption of the proposed AC system with and without the PCM heat exchanger for two cases with different cooling capacities. The results showed that using the PCM heat exchanger increased the partial load ratio, avoiding inefficient operation in both cases. The higher partial load ratio in charge mode increased the SEER to 4.97 from 4.19 (19% increase) in Case 1 and to 4.96 from 3.38 (32% increase) in Case 2. Simultaneously, the total energy consumption was reduced by 11% in Case 1 and 30% in Case 2. These results demonstrate the effectiveness of the proposed system and further suggest its benefits are especially high in situations where relatively large-capacity AC systems are installed.

Funding

This work was funded by JSPS KAKENHI Grant Numbers JP21K18768 and JP24K21646.

Acknowledgements

The authors acknowledge the technical support by MDI Corporation and KANEKA Corporation, and the experimental assistance by Ryoya Hashimoto and Anju Tanaka.

References

[1] International Energy Agency. World Energy Outlook. 2023. Available online: https://www.iea.org/reports/world-energy-outlook-2023 (accessed on 18 April 2025).
[2] Heat Pump and Thermal Storage Technology Center of Japan. Improvement of Efficiency by Inverter Air-Conditioners. Available online: https://www.hptcj.or.jp/e/learning/tabid/364/Default.aspx (accessed on 18 April 2025).
[3] Conti P, Franco A, Bartoli C, Testi D. A design methodology for thermal storages in heat pump systems to reduce partial-load losses. *Appl. Therm. Eng.* 2022; 215: 118971. https://doi.org/10.1016/j.applthermaleng.2022.118971.
[4] Kindaichi S, Kindaichi T. Indoor thermal environment and energy performance in a central air heating system using a heat pump for a house with underfloor space for heat distribution. *Build. Serv. Eng. Res. Technol.* 2022; 43: 755–766. https://doi.org/10.1177/01436244221117356.
[5] Kindaichi S, Nishina D, Murakawa S, Ishida M, Ando M. Analysis of energy consumption of room air conditioners: An approach using individual operation data from field measurements. *Appl. Therm. Eng.* 2017; 112: 7–14. https://doi.org/10.1016/j.applthermaleng.2016.10.017.
[6] ASHRAE. *2020 ASHRAE Handbook HVAC Systems and Equipment*; Chapter 50 Thermal Storage; ASHRAE: Peachtree Corners, GA, USA, 2020; p. 50.1–50.4.
[7] Akeiber H, Nejat P, Majid MZA, Wahid MA, Jomehzadeh F, Famileh IZ, Calautit JK, Hughes BR, Zaki SA. A review on a phase change material (PCM) for sustainable passive cooling in building envelopes. *Renew. Sustain. Energy Rev.* 2016; 60: 1470–1497. https://doi.org/10.1016/j.rser.2016.03.036.
[8] Jamil H, Alam M, Sanjayan J, Wilson J. Investigation of PCM as retrofitting option to enhance occupant thermal comfort in a modern residential building. *Energy Build.* 2016; 133: 217–229. https://doi.org/10.1016/j.enbuild.2016.09.064.
[9] Fabiani C, Piselli C, Pisello AL. Thermo-optic durability of cool roof membranes: Effect of shape stabilized phase change material inclusion on building energy efficiency. *Energy Build.* 2020; 207: 109592. https://doi.org/10.1016/j.enbuild.2019.109592.
[10] Garg H, Pandey B, Saha SK, Singh S, Banerjee R. Design and analysis of PCM based radiant heat exchanger for thermal management of buildings. *Energy Build.* 2018; 169: 84–96. https://doi.org/10.1016/j.enbuild.2018.03.058.
[11] Bogatu DI, Kazanci OB, Olesen BW. An experimental study of the active cooling performance of a novel radiant ceiling panel containing phase change material (PCM). *Energy Build.* 2021; 243: 110981. https://doi.org/10.1016/j.enbuild.2021.110981.
[12] Gholamibozanjani G, Farid M. A comparison between passive and active PCM systems applied to buildings. *Renew. Energy* 2020; 162: 112–123. https://doi.org/10.1016/j.renene.2020.08.007.
[13] Gholamibozanjani G, Farid M. Application of an active PCM storage system into a building for heating/cooling load reduction. *Energy* 2020; 210: 118572. https://doi.org/10.1016/j.energy.2020.118572.
[14] Liu J, Liu Y, Yang L, Liu T, Zhang C, Dong H. Climatic and seasonal suitability of phase change materials coupled with night ventilation for office buildings in Western China. *Renew. Energy* 2020; 147: 356–373. https://doi.org/10.1016/j.renene.2019.08.069.
[15] Solgi E, Fayaz R, Kari BM. Cooling load reduction in office buildings of hot-arid climate, combining phase change materials and night purge ventilation. *Renew. Energy* 2016; 85: 725–731. https://doi.org/10.1016/j.renene.2015.07.028.
[16] Solgi E, Kari BM, Fayaz R, Taheri H. The impact of phase change materials assisted night purge ventilation on the indoor thermal conditions of office buildings in hot-arid climates. *Energy Build.* 2017; 150: 488–497. https://doi.org/10.1016/j.enbuild.2017.06.035.
[17] Türkakar G. Design and optimization of PCM-air cold energy storage device to be used for peak electricity shaving. *J. Therm. Sci. Technol.* 2021; 41: 23–36. https://doi.org/10.47480/isibted.979300.
[18] Nagano K, Takeda S, Mochida T, Shimakura K, Nakamura T. Study of a floor supply air conditioning system using granular phase change material to augment building mass thermal storage—Heat response in small scale experiments. *Energy Build.* 2006; 38: 436–446. https://doi.org/10.1016/j.enbuild.2005.07.010.

[19] Chaiyat N. Energy and economic analysis of a building air-conditioner with a phase change material (PCM). *Energy Convers. Manage.* 2015; 94: 150–158. https://doi.org/10.1016/j.enconman.2015.01.068.
[20] Yu M, Li S, Zhang X, Zhao Y. Techno-economic analysis of air source heat pump combined with latent thermal energy storage applied for space heating in China. *Appl. Therm. Eng.* 2021; 185: 116434. https://doi.org/10.1016/j.applthermaleng.2020.116434.
[21] Tariq SL, Ali HM, Akram MA, Janjua MM, Ahmadlouydarab M. Nanoparticles enhanced phase change materials (NePCMs)—A recent review. *Appl. Therm. Eng.* 2020; 176: 115305. https://doi.org/10.1016/j.applthermaleng.2020.115305.
[22] Sheikholeslami M, Jafaryar M, Shafee A, Li Z. Simulation of nanoparticles application for expediting melting of PCM inside a finned enclosure. *Phys. A Stat. Mech. Its Appl.* 2019; 523: 544–556. https://doi.org/10.1016/j.physa.2019.02.020.
[23] Li Z, Shahsavar A, Al-Rashed AAAA, Talebizadehsardari P. Effect of porous medium and nanoparticles presences in a counter-current triple-tube composite porous/nano-PCM system. *Appl. Therm. Eng.* 2020; 167: 114777. https://doi.org/10.1016/j.applthermaleng.2019.114777.
[24] Sheikholeslami M, Jafaryar M, Shafee A, Babazadeh H. Acceleration of discharge process of clean energy storage unit with insertion of porous foam considering nanoparticle enhanced paraffin. *J. Clean. Prod.* 2020; 261: 121206. https://doi.org/10.1016/j.jclepro.2020.121206.
[25] Riahi S, Saman WY, Bruno F, Belusko M, Tay NHS. Performance comparison of latent heat storage systems comprising plate fins with different shell and tube configurations. *Appl. Energy* 2018; 212: 1095–1106. https://doi.org/10.1016/j.apenergy.2017.12.109.
[26] Souayfane F, Fardoun F, Biwole PH. Phase change materials (PCM) for cooling applications in buildings: A review. *Energy Build.* 2016; 129: 396–431. https://doi.org/10.1016/j.enbuild.2016.04.006.
[27] Kasaeian A, Bahrami L, Pourfayaz F, Khodabandeh E, Yan WM. Experimental studies on the applications of PCMs and nano-PCMs in buildings: A critical review. *Energy Build.* 2017; 154: 96–112. https://doi.org/10.1016/j.enbuild.2017.08.037.
[28] Dubovsky V, Ziskind G, Letan R. Analytical model of a PCM-air heat exchanger. *Appl. Therm. Eng.* 2011; 31: 3453–3462. https://doi.org/10.1016/j.applthermaleng.2011.06.031.
[29] Loem S, Deethayat T, Asanakham A. Kiatsiriroat, T. Study on phase change material thermal characteristics during air charging/discharging for energy saving of air-conditioner. *Heat Mass Transf.* 2020; 56: 2121–2133. https://doi.org/10.1007/s00231-020-02839-4.
[30] Morovat N, Athienitis AK, Candanedo JA, Dermardiros V. Simulation and performance analysis of an active PCM-heat exchanger intended for building operation optimization. *Energy Build.* 2019; 199: 47–61. https://doi.org/10.1016/j.enbuild.2019.06.022.
[31] Stathopoulos N, Mankibi ME, Santamouris M. Numerical calibration and experimental validation of a PCM-Air heat exchanger model. *Appl. Therm. Eng.* 2017; 114: 1064–1072. https://doi.org/10.1016/j.applthermaleng.2016.12.045.
[32] Takeda S, Nagano K, Mochida T, Shimakura K. Development of a ventilation system utilizing thermal energy storage for granules containing phase change material. *Sol. Energy* 2004; 77: 329–338. https://doi.org/10.1016/j.solener.2004.04.014.
[33] Nagano K, Takeda S, Mochida T, Shimakura K, Nakamura T. Study on floor supply air conditioning system storing cold energy for building structure and granules including phase change material: Part 1 Construction of a small-scale experimental system and the thermal characteristics. *J. Environ. Eng.* 2004; 69: 21–28. https://doi.org/10.3130/aije.69.21_2.
[34] Tani K, Kindaichi S, Kawasaki K, Nishina D. Application of a Phase-Change Material Heat Exchanger to Improve the Efficiency of Heat Pump at Partial Loads. *Energies* 2025; 18(14): 3694. https://doi.org/10.3390/en18143694.
[35] ASHRAE. *2017 ASHRAE Handbook Fundamentals*; Chapter 4 Heat Transfer; ASHRAE: Peachtree Corners, GA, USA, 2017; p. 4.25.
[36] Government Buildings Department, MLIT. LCEM Tool Ver 3.10. Available online: https://www.mlit.go.jp/gobuild/sesaku_lcem_lcemtool_index.htm (accessed on 25 May 2025).
[37] Institute for Built Environment and Carbon Neutral for SDGs. The Best Program Sample Data for an 8-Zone Office on a Standard Floor. Available online: http://ibec.or.jp/best/english/program/pdf/manual/try_best20090801_2.pdf (accessed on 25 May 2025).